Reducing Disorder in Artificial Kagome Ice

Stephen A. Daunheimer, Olga Petrova, Oleg Tchernyshyov, and John Cumings

Reducing Disorder in Artificial Kagome Ice

Stephen A. Daunheimer,[1] Olga Petrova,[2] Oleg Tchernyshyov,[2] and John Cumings[1,*]

[1]*Department of Materials Science & Engineering, University of Maryland, College Park, Maryland 20742, USA*
[2]*Department of Physics & Astronomy, Johns Hopkins University, Baltimore, Maryland 21218, USA*
(Dated: August 25, 2011)

Artificial spin ice has become a valuable tool for understanding magnetic interactions on a microscopic level. The strength in the approach lies in the ability of a synthetic array of nanoscale magnets to mimic crystalline materials, composed of atomic magnetic moments. Unfortunately, these nanoscale magnets, patterned from metal alloys, can show substantial variation in relevant quantities such as coercive field, with deviations up to 16%. By carefully studying the reversal process of artificial kagome ice, we can directly measure the distribution of coercivities, and by switching from disconnected islands to a connected structure, we find that the coercivity distribution can achieve a deviation of only 3.3%. These narrow deviations should allow the observation of behavior that mimics canonical spin-ice materials more closely.

Water ice and spin ice are classic examples of geometrically frustrated systems [1, 2], both with residual low-T entropy [3]. In water ice, thermodynamic phases with ordered protons were discovered after decades of experiments [4]. In contrast, no dipole-ordered phase has been observed in spin ice even at the lowest accessible temperatures, contrary to a theoretical prediction [5]. Divergent relaxation times and quenched disorder in samples have been cited as possible explanations. Artificial spin ice has been proposed to help address these questions [6], as it allows the direct control of the geometry of the lattice, with the combined ability to directly image the resulting microstate. Here, samples are composed of lattices of nanoscale ferromagnetic islands, where the magnetization of each element points along its longitudinal axis. At the vertices of the lattice, the ferromagnetic elements interact, and because of the geometry of the system, their magnetic configurations are frustrated [6–11]. This allows the study of frustration in systems where crystalline imperfections can be completely removed by design, or introduced in a controlled way. Unfortunately, current lithographic techniques are limited by unintended roughness at edges and interfaces, creating inadvertent disorder. This diminishes the ability to compare observations from artificial spin ice materials with studies of spin ice oxides, where magnetic atoms are presumed to be identical.

Edge roughness of nanomagnetic elements is known to substantially influence the coercive field, by creating nucleation sites that can initiate the magnetic reversal [12]. In some artificial spin ice geometries, this edge roughness can create a large variability in the behavior of the artificial "atoms" (magnetic nano-islands). In recent studies of artificial kagome ice, the variations in coercivity were found to be substantial—up to 16% of the average coercive value [8, 9, 13]. This variability can easily be reduced by choosing materials with low crystal anisotropy [9], but we here show substantial further reduction with a geometry with connected magnetic islands. In a connected geometry, nontrivial spin textures (domain walls) already exist at the vertices even in equilibrium, and thus the reversal process is not dictated by the nucleation of new domain walls, a step that is more susceptible to the effects of edge roughness.

To address the problem of disorder and variability in artificial ice, techniques must first be established to measure the static disorder in the material, a problem that is complicated by the sought-after occurrence of statistical disorder, in analogy with thermal disorder in pyrochlore spin ice. Prior work has addressed this problem by focusing on the reversal of artificial kagome ice in an external field applied at 180° to the direction of initial magnetization [8, 9], a potentially deterministic process, in which statistical variations are hopefully minimized. However, the reversal process under these conditions shows large discrete avalanche events, and for the materials with small static disorder described below, the variations in these reversals are almost entirely dominated by non-reproducible statistical disorder. Prior studies provided disorder estimates as large as 16% through Monte Carlo modeling of the 180° reversal process, but this approach is not possible when the amount of quenched disorder is much smaller.

In this Letter, we present a method to alleviate this issue by performing reversals with the field applied at 120° and 100° to the direction of initial magnetization instead of 180°. Under these conditions, magnetization reversal in individual islands proceeds largely independently of their neighbors, preventing the formation of avalanches. This enables us to extract the spread of coercivities directly from the magnetization curves $M(H)$. These data are then used to calculate a disorder parameter, $\sigma/\overline{H_c}$, where $\overline{H_c}$ is the average coercive field of a magnetic element and σ is the standard deviation of the distribution. Using this parameter, we are able to directly compare our data with those from other groups. By considering carefully the magnetic reversal process, we demonstrate that this disorder parameter can be greatly reduced in a system with connected magnetic islands. Additionally, all data used to determine the disorder present in a crystal

can be obtained directly from experiments rather than relying on parameters extracted from Monte Carlo simulations.

In our studies, we choose the kagome lattice for our artificial spin ice [8–11], as shown in Fig. 1(a) and 1(b). Samples were patterned via e-beam lithography onto an electron transparent SiN membrane with PMMA resist [11]. The $Ni_{80}Fe_{20}$ films were deposited by e-beam evaporation followed by metal lift-off. The resulting elements are 500 nm long, 110 nm wide, and 23 nm thick with an additional 4 nm capping layer of Al to prevent oxidation. Reversals were performed *in situ* in a transmission electron microscope in Lorentz mode to capture the magnetic configuration of the crystal throughout a reversal. A magnified image of a portion of the sample can be seen in Fig. 1(a). Magnetic reversal in this system can be described in terms of the emission, propagation, and absorption of domain walls carrying non-zero magnetic charge [14]. Similar emergent magnetic monopole excitations have been shown to exist in both conventional [15–20] and artificial spin ice [8, 9].

The nature of magnetic charges is understood as follows. Because magnetic induction $\mathbf{B} = \mu_0(\mathbf{H} + \mathbf{M})$ is divergence-free, a region where lines of magnetization $\mathbf{M}$ terminate or originate becomes a source of sink of magnetic field $\mathbf{H}$. Thus magnetic charges in artificial spin ice contain integer multiples of the magnetization flux of a single magnetic element. In these units, a monopole propagating along an element during reversal can carry a charge ± 2, and a vertex can carry a charge of ± 1 or ± 3. The interactions between the charges via $\mathbf{H}$ can be described simply in terms of a Coulomb potential [14]. Triple charges represent ice-rule violations for the kagome lattice, and although they have been observed experimentally during 180° reversals in other systems [8, 9], they *never* appear in the low-disorder system we study here [11].

Before considering the angle dependence, it is instructive to consider the microscopic details of the reversal process, depicted in Figure 1(c). In panel (i), the horizontal element will be the first to reverse because the external magnetic field has the largest component along its axis. The reversal begins with the emission of a domain wall of $+2$ charge into the horizontal element, leaving behind a vertex with -1 charge. The domain wall moves along the element until it reaches the opposite vertex, thereby reversing the element's magnetization. In panel (iii), the vertex with charge -1 pulls the domain wall with charge $+2$ in, thereby changing its own charge to $+1$. The reversal is different for the disconnected lattice where a domain wall needs to be nucleated at the end of an element, rather than emitted from a vertex. In this case, the field required to inject a charged domain wall can vary significantly depending on crystal symmetry and edge roughness of the elements.

One might expect the magnitude of the coercive field

to be lowest when the field is parallel to the element receiving the emitted domain wall: only the longitudinal component of the magnetic field pushes a domain wall along the element. However, in a connected lattice, the transverse field component also plays a role, thanks to an asymmetric distribution of magnetic charge within each vertex.

Consider a simplified model of a vertex consisting of three thin domain walls meeting at the center of the vertex, Fig. 2. In a vertex with unit charge, two of the walls are neutral (head-to-tail) and one is magnetically charged (head-to-head or tail-to-tail). An applied field exerts a maximum force on the charged domain wall when it is applied normal to the wall, or at 30° to the axis of the element receiving the wall. Micromagnetic simulations confirm these qualitative considerations [14]. The coercive field depends on its orientation as follows:

$$H_c(\theta_i) = H_c^i / |\cos(\theta_i + \alpha)|. \tag{1}$$

Here θ_i is the angle of the applied field with the long axis of the ith element, H_c^i is the minimum coercivity of that element, and $\alpha = 19°$ is an offset angle [14].

Using this model, we measure the disorder in our artificial ice, as caused by variability in the coercive field of the elements, by performing magnetic reversals of large arrays with more than 10^4 elements. The system is initially magnetized in a high field $H \gg \overline{H_c}$. The field is switched off and the sample is rotated through the desired angle θ in its plane. In this Letter, we focus on $\theta = 100°$ and 120°. As can be seen from Eq. (1), these orientations guarantee large differences in the coercive fields for different sublattices and lead to avalanche-free reversal. This allows us to extract reversal statistics for both sublattices during the reversal process.

During reversal, the field is increased in steps of 5.0 Oe, and since it can also effect the Lorentz imaging, the field must be reduced to 0 after each step, to capture an image at remanence. Images are then run through a MATLAB script that automatically determines the magnetic configuration of each element; one image will give us one point on the $M(H)$ plot, as shown in the top panel of Fig. 3. These results can then be compared with numerical simulations of an array of interacting elements as described previously [14]. Simulated curves $M(H)$ for a Gaussian distribution of coercive fields with $\sigma / \overline{H_c} = 5\%$ are shown in the bottom panel of Fig. 3. Details of the simulations will be described elsewhere [21].

To determine the disorder in our crystals directly, we fit the $M(H)$ curves to the expected cumulative distribution function, a superposition of error functions in the case when coercive fields have Gaussian statistics:

$$M_x(H) = \sum_i m_i \operatorname{erf}\left(\frac{H - \overline{H_c^i}}{\sigma_i \sqrt{2}}\right), \tag{2}$$

where M_x is the magnetization along the initial polarization direction, i indexes the sublattices in order of re-

versal, m_i is the amount of magnetic moment carried by the sublattice, $\overline{H_c^i}$ is the average coercive field, and σ_i is the standard deviation. From fitting the reversal at $\theta = 100°$, we obtain a disorder parameter, $\sigma_1/\overline{H_c^1} = 3.3\%$, from the values $\overline{H_c^1} = 347$ Oe and $\sigma_1 = 11.3$ Oe. The second plateau at $\theta = 100°$ gives a slightly higher disorder parameter of 4.7%, from $\overline{H_c^2} = 915$ Oe and $\sigma_2 = 43.3$ Oe. We believe this is due to a rotational disorder from element-to-element in the lattice, as expressed by the α offset parameter from Equation (1). Disorder in α should not be expected to contribute to σ_i when $|\cos(\theta_i + \alpha)| \approx 1$, which occurs for σ_1 near $\theta = 100°$ in our system. When $\theta_i \approx \pm 90°$, the coercivity diverges and even small rotational disorder would be expected to cause substantial variations. From the reversal at $\theta = 120°$ degrees, we obtain $\sigma_1/\overline{H_c^1} = 3.7\%$, and $\sigma_2/\overline{H_c^2} = 4.6\%$, confirming the trend of minimum disorder near the minimum H_c^i, and increasing monotonically with θ away from that point. We note that the reversals at $\theta = 180°$ have a different character. They involve magnetic avalanches in which long chains of links reverse together. We plan to address this question in a separate publication.

From this, we find that the static disorder is very low in our samples, 3.3%, which is a factor of 4-5 smaller than values for other systems [8, 9]. This low amount of disorder is a result of the geometry of our connected elements. Here, charged domain walls always exist at the vertices, even at remanence. For a given magnetic configuration, there is very little change in the location and angle of the charged wall throughout the sub-lattice. The same is not true for a disconnected lattice. The process of nucleating and injecting a domain wall is more sensitive to quenched disorder in disconnected lattices, as the ± 2 domain walls must be nucleated from the end of one of the elements instead of simply injected, and any significant edge roughness may influence the nucleation process. This leads to an increase in the width of the static disorder for a disconnected lattice.

We summarize the effect of the connected lattice on the disorder in Table I, where we compare $\sigma/\overline{H_c}$ with two other experimental results, using different materials [8] and disconnected geometry [9]. The effect of the connected geometry is to decrease the disorder from 13% to 3.3%. We acknowledge that the connected lattice presented herein and the disconnected lattice used for comparison have been fabricated by different research groups, but we have also performed simulations that support the relative difference. These micro-magnetic calculations were performed using the OOMMF software package from NIST [22]. Simulations were carried out for 180° reversals on Y-junctions with random edge roughness, comparable to the fabricated structures, and the results from an ensemble of calculations are also shown in Table I, exhibiting a similar relative relationship.

In addition to the lattice geometry, the material used in the fabrication of the crystal is important. Our crys-

tals and most other artificial spin ices have been made using $Ni_{80}Fe_{20}$, which has a low crystal anisotropy, giving polycrystal films with uniform magnetic properties. This is not the same for cobalt, as used in [8], which has a strong hexagonal anisotropy. Magnetic elements fabricated from polycrystal Co films would be expected to have a broad distribution of coercivities.

By using a connected lattice of $Ni_{80}Fe_{20}$ elements, we have alleviated both of these problems and created crystals with low disorder. Our crystal geometry is ideal in that it allows for a more accurate representation of spin ice in frustrated magnetic materials. For example, unlike other systems [8, 9], the low-disorder system described herein rigorously obeys its corresponding set of ice rules, a desirable feature given the interaction energy of approximately 10^4 K [6]. This presents the system as a more ideal model of frustration, providing the hope of addressing outstanding problems, such as the occurrence of a possible ground state in kagome ice [23, 24].

* Corresponding author, cumings@umd.edu

[1] H. T. Diep, *Frustrated Spin Systems* (World Scientific Publishing Co. Pte. Ltd., 2004).

[2] C. Lacroix, P. Mendels, and F. Mila, eds., *Introduction to frustrated magnetism*, vol. 164 of *Springer series in solid-state sciences* (Springer, 2011).

[3] A. P. Ramirez, A. Hayashi, R. J. Cava, R. Siddharthan, and B. S. Shastry, Nature **399**, 333 (1999).

[4] V. F. Petrenko and R. W. Whitworth, *Physics of Ice* (Oxford University Press, 1999).

[5] R. Melko, B. den Hertog, and M. Gingras, Phys. Rev. Lett. **87** (2001).

[6] R. Wang, et al., Nature **439**, 303 (2006).

[7] J. P. Morgan, A. Stein, S. Langridge, and C. H. Marrows, Nature Phys. **7**, 75 (2011).

[8] S. Ladak, D. E. Read, G. K. Perkins, L. F. Cohen, and W. R. Branford, Nature Phys. **6**, 359 (2010).

[9] E. Mengotti, L. J. Heyderman, A. F. Rodriguez, F. Nolting, R. V. Huegli, and H.-B. Braun, Nature Phys. **7**, 68 (2011).

[10] M. Tanaka, et al., Phys. Rev. B **73**, 052411 (2006).

[11] Y. Qi, T. Brintlinger, and J. Cumings, Phys. Rev. B **77**, 094418 (2008).

[12] J. Gadbois and J.-G. Zhu, IEEE Trans. Magn. **31**, 3802 (1995).

[13] K. K. Kohli, A. L. Balk, J. Li, S. Zhang, I. Gilbert, P. E. Lammert, V. H. Crespi, P. Schiffer, and N. Samarth, ArXiv e-prints (2011), 1106.1394.

[14] P. Mellado, O. Petrova, Y. Shen, and O. Tchernyshyov, Phys. Rev. Lett. **105**, 187206 (2010).

[15] C. Castelnovo, R. Moessner, and S. L. Sondhi, Nature **451**, 42 (2008).

[16] I. Ryzhkin, J. Exp. Theor. Phys. **101**, 481 (2005).

[17] L. D. C. Jaubert and P. C. W. Holdsworth, Nature Phys. **5**, 258 (2009).

[18] D. J. P. Morris, et al., Science **326**, 411 (2009).

[19] T. Fennell, et al., Science **326**, 415 (2009).

[20] S. T. Bramwell, et al., Nature **461**, 956 (2009).

[21] Y. Shen, O. Petrova, P. Mellado, S. Daunheimer, J. Cumings, and O. Tchernyshyov, (unpublished).

[22] M. J. Donahue and D. G. Porter, Tech. Rep. 6376, NIST, Gaithersburg, MD (1999), http://math.nist.gov/oommf.

[23] G. Möller and R. Moessner, Phys. Rev. B **80** (2009).

[24] G.-W. Chern, P. Mellado, and O. Tchernyshyov, Phys. Rev. Lett. **106**, 207202 (2011).

FIGURES

FIG. 1. (a) In-focus TEM image of the artificial kagome ice. Lines representing the kagome planes are overlaid to show how the origin of the honeycomb structure of our crystals. (b) Lorentz contrast image of the kagome lattice. The contrast difference can clearly be seen with a bright and dark edge across each element in the array. The magnetization of six elements is shown along with the resulting charge at the vertex they are connected to. Inset: the intensity profile along the indicated black line. The magnetization of two elements is captured in the profile and depicted by arrows on the Lorentz image and on the profile itself. (c) A cartoon of the reversal process of an individual element is shown in panels (i)-(iv), as described in the text.

FIG. 2. Illustration of the crystal magnetization at the beginning of a $\theta = 120°$ reversal. The table shows values of θ_i for the elements of the three sublattices. The angles are with respect to H_{app}. The red lines at the vertices indicate the location of a head-to-head or tail-to-tail domain wall which is the source of magnetic charge at each vertex.

FIG. 3. Experimental (top) and theoretical (bottom) results of a uniaxial reversal along $100°$, $120°$, and $180°$. Solid lines in the experimental results are fits of a superposition of error functions used to extract the reversal statistics for each sublattice.

TABLES

	σ_1/H_c^1	Composition & Structure
Experiment	0.167	Co, connected [8]
	0.130	NiFe, disconnected [9]
	0.033	NiFe, connected, this work
OOMMF Simulations	0.040	NiFe, connected
	0.089	NiFe, disconnected

TABLE I. Experimental reversal results and their associated disorder. Theoretical results are shown for comparison. Theoretical results are averaged over 10 different simulations for each lattice.
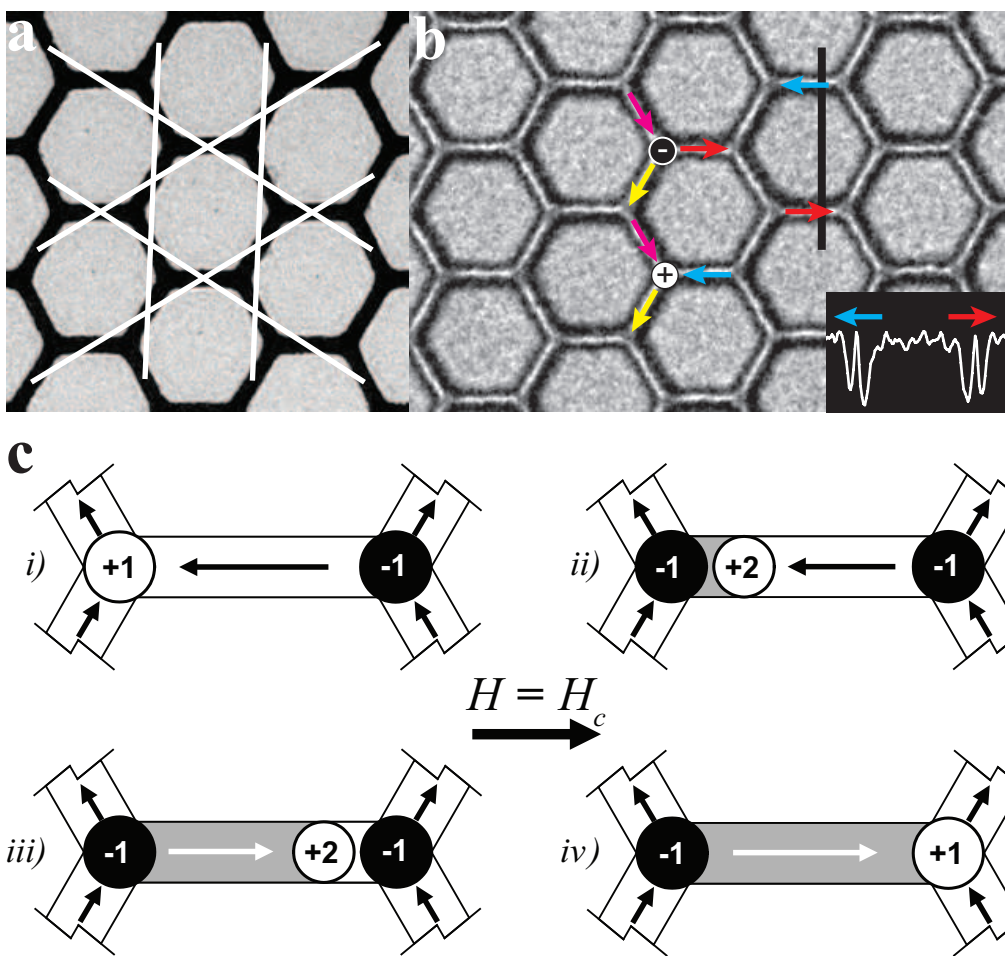
Figure 1   LD13350   25Aug2011

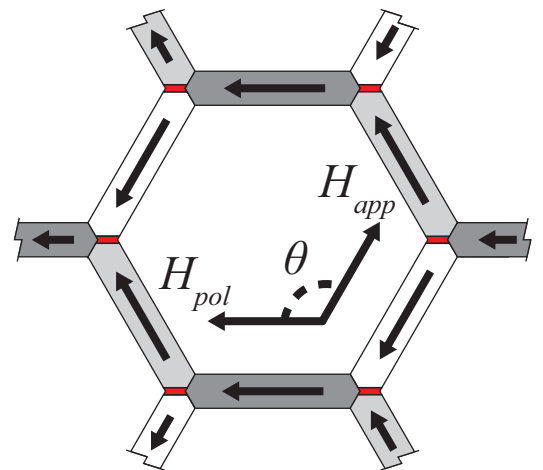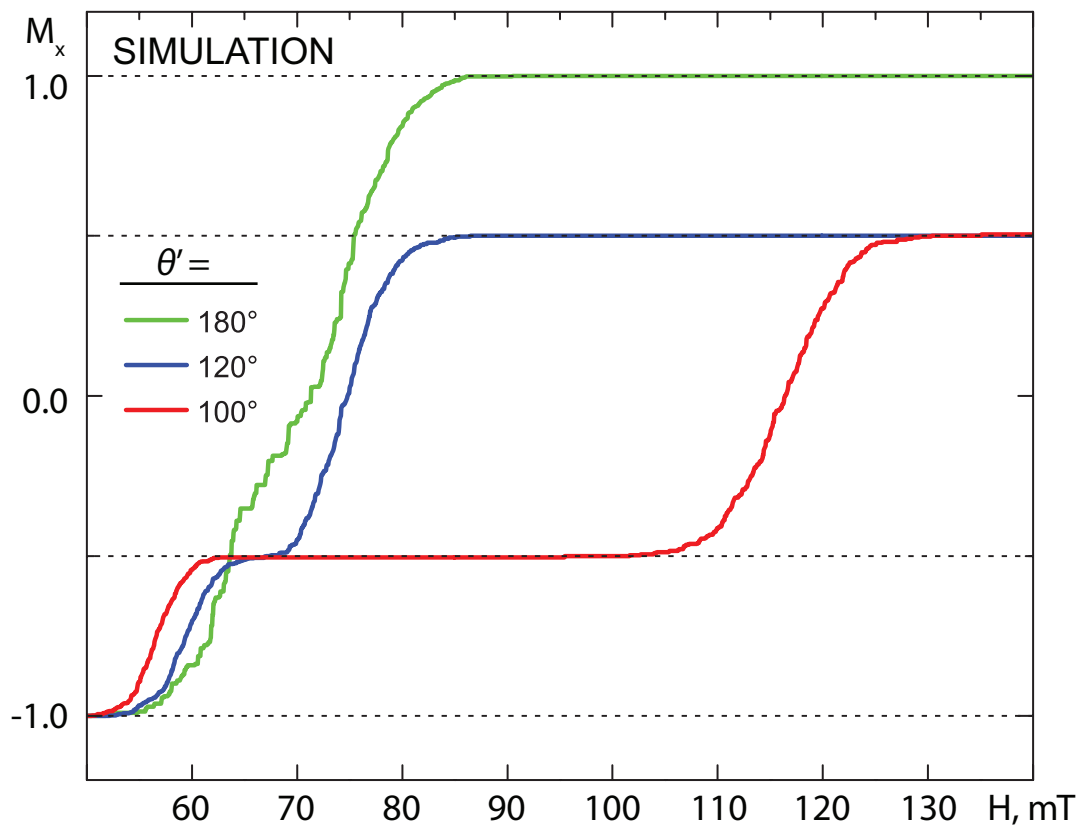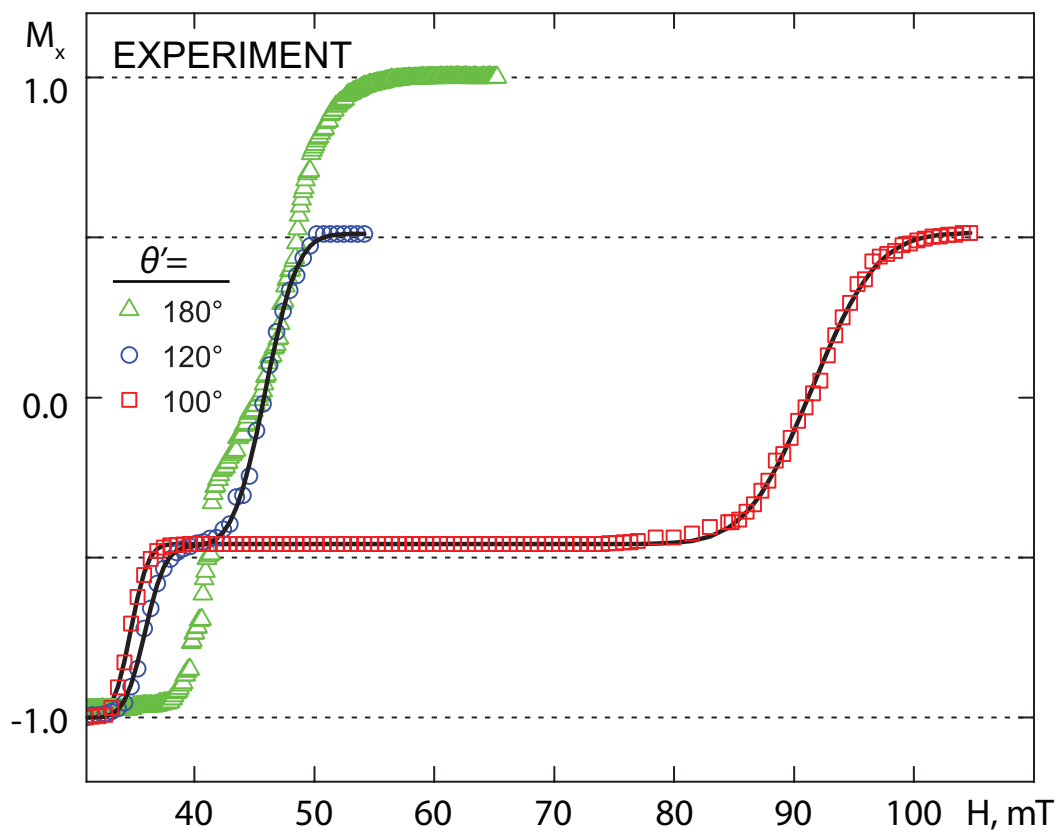| Lattice	θ_i	
	$\theta = 100°$	$\theta = 120°$
☐	160°	180°
◼ (dark gray)	100°	120°
◻ (light gray)	40°	60°

Figure 2   LD13350   25Aug2011

Figure 3   LD13350   25Aug2011